Cellulose (2023) 30:4197–4213
https://doi.org/10.1007/s10570-023-05127-6

ORIGINAL RESEARCH

Influences on the accuracy of crystallinities determined by the method of Ruland and Vonk

Daniel Van Opdenbosch

Received: 27 October 2022 / Accepted: 3 March 2023 / Published online: 30 March 2023

Abstract X-ray diffractometry is the method of choice for the determination of crystallinities in non-thermoplastic polymers, prominently in cellulose. Obtaining quantitative measures on a sound theoretical basis includes the integration of intensities scattered by the crystalline phase over volume elements in reciprocal space. This is hampered by the occurrence of diffuse scattering, whose profile is not readily distinguishable from scattering by amorphous phases. The manner of evaluating diffractograms pioneered by Ruland and refined by Vonk allows to determine crystallinities by integrating only the coherently scattered portion of crystalline-phase intensities and extrapolating their proportion to a scattering vector of 0. However, preferred crystallite orientations within measured samples, as well as the range of scattering vectors from which the data are extrapolated, have been pointed out as sources of systematic error. We investigated the influence of these factors at the examples of two crystalline structures of cellulose and two types of technically relevant thermoplastics. We found that the method of Ruland and Vonk is rather robust when applied to cellulose, but decidedly less so when applied to polymers with highly symmetric crystalline phases. We also found that there is a range of scattering vectors that leads systematically to the most accurate measures of crystallinity. We further investigated the influence of the crystallite sizes, the crystallinities themselves and the thermal displacement factors, and found that the latter had a profound effect on the accuracies of determined crystallinities.

Introduction

Thermocalorimetry is arguably the gold standard for the determination of crystallinities (also 'degree of crystallization') in polymers, under the assumption of a known specific heat of fusion of the crystalline phase – if the crystallites can be molten. A complementary method is X-ray diffractometry, which provides additional structural information, typically at the expense of a more elaborate data analysis, and under a larger set of assumptions. The latter is widely applied to polymer materials in which thermal degradation precedes melting processes. Unsurprisingly, it was first applied to determine crystallinities in the technologically relevant material families rubber (Gehman and Field 1939) and, even earlier, cellulose (Clark 1930).

Methods based on X-ray diffractometry rely on the deconvolution of recorded data, and its attribution to different portions of the material. We refer

Supplementary Information The online version contains supplementary material available at https://doi.org/10.1007/s10570-023-05127-6.

D. V. Opdenbosch (✉)
Campus Straubing for Biotechnology and Sustainability, Chair for Biogenic Polymers, Technical University of Munich, Schulgasse 16, 94315 Straubing, Germany
e-mail: daniel.van-opdenbosch@tum.de

to Riello (2004) for a comprehensive introduction to quantitative crystallinity analyses in semi-crystalline polymers and presuppose knowledge about the meaning of the terms in Bragg's law and the Laue equations. In brief, recorded elastically scattered X-ray diffractometry data consist of directional intensities that can be grouped as follows:

- Coherent scattering. These are the eponymous diffracted waves, arising from the crystalline portion as discrete intensity maxima, termed Bragg peaks or -reflexes, by collective interference.
- Incoherent scattering. All else: Amorphous scattering from the portion of the material not exhibiting crystalline order. Continuous intensities, therefore grouped as incoherent, even though short-range order gives rise to broad intensity maxima. Background scattering from the instrumental setup, e.g. from air, or slit edges. Continuous intensities, typically strongly increasing at very low scattering angles, can be reduced by slits or screens and also be measured separately & subtracted. Depending on the setup, scattering from the sample holder may also be recorded and may include diffraction peaks. Diffuse scattering from the crystalline portion, arising from disturbed interference conditions, e.g. by thermal motions or structural defects. Continuous intensities, gradually increasing with increasing scattering angle.

The above listing is not exhaustive. For example, the special case of scattering from paracrystalline portions is ignored, as are inelastically scattered photons (relevant on machines without appropriate filter or energy-sensitive detector). However, it covers the most widely encountered contributions, which may be memorized as the **a**morphous, **b**ackground, **c**oherent, and **d**iffuse portions of the data.

Throughout the following, we assume that data was recorded using fixed apertures and has been corrected for contributions from the instrumental setup. For simplicity, we restrict ourselves to homopolymeric materials (as commented upon in Discussion) consisting of amorphous and crystalline regions.

In case of isotropic scattering from samples without preferred orientations, if one were able to correctly assign portions of the data as stemming from these two types of regions, the mass fraction of the crystalline phase x_c of the sample could be calculated by a fraction of invariant integrals, Eq. (1) (Riello 2004).

$$x_c = \int_0^\infty I_c(s)s^2\,\mathrm{d}s \Big/ \int_0^\infty I(s)s^2\,\mathrm{d}s \tag{1}$$

Here, $I_c(s)$ and $I(s)$ are the intensities scattered from the crystalline phase and the total intensities as a function of the magnitude of the scattering vector $s = |\mathbf{s}| = 2\sin\theta/\lambda$. However, the diffuse scattering portion of the data is not readily distinguishable from amorphous scattering, yet arises from the crystalline portion. As worded by Riello (2004), "[t]he main problem [in deconvolution] is the separation of the scattering of the amorphous phase from the global smooth background of the pattern of the semicrystalline sample".

This problem can be ignored, if one is content with a semiquantitative method to determine crystallinity indices, e.g. the widely applied Segal (1959) peak height ratio method, or a straightforward integrated area ratio (Yao et al. 2020). In the following, we outline that it hinges on the rate by which intensities are attenuated from the Bragg reflexes into the global smooth background, and how the need for an explicit separation can be circumvented.

Attenuations are generally described by the application of a factor $D(s)$, Eq. (2). If the interference conditions are disturbed predominantly by thermal oscillations, the Debye-Waller factor (3) provides a suitable description. While thermal motions may be described in great detail, down to directional measures $\mathbf{u}$ for each atom in the unit cell, a single averaged measure $k = \langle|\mathbf{u}|^2\rangle$ is typically sufficient for the purpose of determining polymer crystallinities.

$$\int_0^\infty I_{coh}(s)s^2\,\mathrm{d}s = x_c \int_0^\infty \langle f^2(s)\rangle D(s)s^2\,\mathrm{d}s \tag{2}$$

$$D(s) = \exp(-ks^2) \tag{3}$$

Here, $I_{coh}(s)$ are the intensities solely contained within the Bragg peaks. $\langle f^2(s)\rangle$ is the average of the squared atomic scattering factors, equalling the total intensities:

$$\int_0^\infty I(s)s^2\,\mathrm{d}s = \int_0^\infty \langle f^2(s)\rangle s^2\,\mathrm{d}s \tag{4}$$

Equation (4) in (1) gives:

$$\int_0^\infty I_\mathrm{c}(s)s^2\,\mathrm{d}s = x_\mathrm{c}\int_0^\infty \langle f^2(s)\rangle s^2\,\mathrm{d}s \tag{5}$$

Since $I(s) = I_\mathrm{am}(s) + I_\mathrm{c}(s)$, i.e. the sum of intensities scattered from the amorphous and crystalline phases:

$$\int_0^\infty I_\mathrm{am}(s)s^2\,\mathrm{d}s = (1-x_\mathrm{c})\int_0^\infty \langle f^2(s)\rangle s^2\,\mathrm{d}s \tag{6}$$

And since $I_\mathrm{c}(s) = I_\mathrm{coh}(s) + I_\mathrm{diff}(s)$, i.e. the sum of coherent and diffuse scattering:

$$\int_0^\infty I_\mathrm{diff}(s)s^2\,\mathrm{d}s = x_\mathrm{c}\int_0^\infty \langle f^2(s)\rangle(1-D(s))s^2\,\mathrm{d}s \tag{7}$$

This proportionality to $1 - D(s)$ was stated from the outset (Debye 1913). Grouping the intensities $I_\mathrm{am}(s)$ and $I_\mathrm{diff}(s)$ as incoherent scattering $I_\mathrm{inc}(s)$:

$$\begin{aligned}\int_0^\infty I_\mathrm{inc}(s)s^2\,\mathrm{d}s &= \int_0^\infty [I_\mathrm{am}(s) + I_\mathrm{diff}(s)]s^2\,\mathrm{d}s\\ &= \int_0^\infty \left[(1-x_\mathrm{c})\langle f^2(s)\rangle + x_\mathrm{c}\langle f^2(s)\rangle(1-D(s))\right]s^2\,\mathrm{d}s\\ &= \int_0^\infty \langle f^2(s)\rangle(1-x_\mathrm{c})\left[1 + \frac{x_\mathrm{c}(1-D(s))}{1-x_\mathrm{c}}\right]s^2\,\mathrm{d}s\\ &= \int_0^\infty \langle f^2(s)\rangle(1-x_\mathrm{c}D(s))s^2\,\mathrm{d}s\end{aligned} \tag{8}$$

Due to the factor $1 - x_\mathrm{c}D(s)$ in Eq. (8), the separation line between the amorphous and the diffuse scattering is itself dependent on x_c, as intuitively expected.

In the original method of Ruland (1961), $I(s)$ is segmented as $s_0 < s < s_p$, where the lower limit s_0 remained constant, e.g. $s_0 = 0.1$ Å^{-1}, and the upper limit s_p varied, e.g. $s_p = [0.3, 0.6, 0.9, 1.25]$ Å^{-1}. Then, the $D(s)$ are determined, for which the following expression yields the same x_c for all s_p:

$$x_\mathrm{c} = \int_{s_0}^{s_p} I_\mathrm{coh}(s)s^2\,\mathrm{d}s \Big/ \int_{s_0}^{s_p} I(s)s^2\,\mathrm{d}s \cdot K(s_p) \tag{9}$$

$$K(s_p) = \int_{s_0}^{s_p} \langle f^2(s)\rangle s^2\,\mathrm{d}s \Big/ \int_{s_0}^{s_p} \langle f^2(s)\rangle D(s)s^2\,\mathrm{d}s \tag{10}$$

This is achieved by iterating over values of k, which alters $D(s)$ via (3). Considering (4), Eqs. (9) & (10) appear to simply be (2) rearranged, with altered integration limits. However, the presence of Bragg peaks in $I_\mathrm{coh}(s)$ and $I(s)$ makes the inclusion of the terms from (4) non-redundant.

Vonk (1973) further developed Ruland's method, eliminating the iterative search for k by rearranging Eq. (9) as $x_\mathrm{c} = K(s_p)/R(s_p)$ and setting $s_0 := 0$, leaving only the upper cumulative integration limit s_p variable:

$$R(s_p) = \int_{s_0}^{s_p} I(s)s^2\,\mathrm{d}s \Big/ \int_{s_0}^{s_p} I_\mathrm{coh}(s)s^2\,\mathrm{d}s \tag{11}$$

He outlined that, since $K(s_p) \approx 1 + s_p^2 k/2$, a plot of $R(s_p)$ over s_p^2 should oscillate about a straight line $y(s_p^2) = (1 + s_p^2 k/2)/x_\mathrm{c}$ (Vonk 1973). To allow for possible effects of second order lattice defects (i.e. paracrystalline order), which alter the function $D(s)$, Vonk proposed describing $y(s_p^2)$ as a second order polynomial function. x_c and k are then determined by Eqs. (12) and (13).

$$x_\mathrm{c} = 1/y(0) \tag{12}$$

$$k = 2x_\mathrm{c}y'(0) \tag{13}$$

The method of Vonk appears to us to be the most efficient way to carry out fully quantitative and theoretically sound determinations of crystallinities. It has been covered in reviews on the matter (Riello 2004; Driemeier and Calligaris 2011) and has been applied repeatedly to the prominent case of cellulosic materials (Fink et al. 1985; Sao et al. 1994; Thygesen et al. 2005). However, two issues present themselves.

The first issue is related to preferred orientations and was already pointed out by Ruland: For oriented samples, the recorded $I_\mathrm{coh}(s)$ and therefore also the $I(s)$ correspond to Eqs. (2) & (4) only after

randomization of the recorded intensities per scattering vector $I(\mathbf{s})$ over all solid angles in reciprocal space ω (Ruland 1961). This is, of course, only possible if the corresponding data is recorded. In basic Bragg-Brentano measurements, i.e. without "the aid of either a texture goniometer or flat-film exposures" (Vonk 1973), it may not be accessible. Then, "[n]on-random orientation of the crystallites in the samples may give rise to systematic errors." (Vonk 1973)

The second issue is the range of cumulative integration limits over which the function $y(s_p^2)$ should be fitted to $R(s_p^2)$, as commented upon by Vonk (1973): Due to the typical presence of strong Bragg peaks at low s, "special consideration must be given to the points at low s_p^2 values, which may be scattered very widely about the y curve." He advised "that in the curve-fitting procedure a lower limit must be set to s_p^2 which is preferably taken higher than the s^2 value corresponding to the second crystalline peak in the diagram. Choosing various lower limits one can obtain an idea as to the accuracy of the extrapolation of y to $s_p^2 = 0$." (Vonk 1973)

We endeavoured to systematically study the effects of preferred orientation and the choice of the lower limit to the range of s_p on the accuracy of x_c, as calculated on the basis of standard Bragg-Brentano data. Specifically, we hypothesized that:

H1 The errors on x_c incurred by preferred orientation are larger, the more symmetrical the crystal structure.
H2 There is a lower limit to the range of s_p that systematically yields the most accurate x_c.
H3 The attenuation rate of the coherently scattered intensities has a systematic influence on the accuracy of x_c. H3.1 This influence correlates with the measure of preferred orientation, H3.2... and with the choice of the range of s_p.
H4 The crystallite sizes and crystallinities have no influence on the accuracy of x_c.

We consider the above hypotheses of particular relevance with regard to the determination of crystallinity in cellulosic materials: Since these –particularly from native cellulose I– typically exhibit preferred orientation, they can be expected to be prone to systematic errors in estimating x_c. On the other hand, they exhibit a low crystal symmetry, as expressed by their large triclinic or moonoclinic unit cells. Knowledge about systematic influences on x_c may aid in choosing the range of s_p, and determining the error on given estimates.

In the current work, we therefore simulated Bragg-Brentano powder diffractograms of cellulose in I α and II structures, while varying the parameters relevant to answer the hypotheses H1 through H4. For comparison, and to systematically test H1, we also simulated diffractograms of two further technical polymers poly(3-hydroxybutyrate) and poly(ethylene). We determined the corresponding x_c using the method of Ruland and Vonk, and performed a series of statistical evaluations on the matrix of parameters and results, both comprehensively and for each material separately.

Experimental

Due to its ubiquity, we decided to simulate data from a Bragg-Brentano diffractometer employing copper Kα $_1$ radiation at a wavelength $\lambda = 1.5406$ Å, using the xrayutilities collection of routines (Kriegner et al. 2013). The simulated data lacked some machine-related features such as scattering from air or slits, or sample offset, while accounting for the line profiles from a typical setup. Out of these three examples, only scattering arising from the setup would have to be corrected for accuracy. The simulated data also lacked intensities from inelastic Compton scattering, which required corrections during Ruland's and Vonk's times (Ruland 1961; Vonk 1973), but is typically filtered from the data recorded on state-of-the-art machines employing energy-sensitive detectors. All data were simulated over the scattering angle range $0° < 2\theta < 180°$.

As a basis for the simulation of the diffractograms from semicrystalline polymer materials, four crystalline phases were selected:

- Cellulose I α (Cell I α), as published by French (2014), as an example for a 'low' triclinic $P1$ symmetry, an intermediate $V = 333$ Å^3 unit cell and large number of Bragg reflexes: Excluding symmetry-equivalents, 1524 observable with copper Kα $_1$ radiation.
- Cellulose II (Cell II), as published by French (2014), as an example for an 'intermediate' mon-

oclinic $P121$ symmetry, a large $V = 671$ Å^3 unit cell and intermediate number of Bragg reflexes: 1026 observable.
- Poly(3-hydroxybutyrate) α (PHB), as published by Wang and Tashiro (2016), as as example for a 'high' orthorhombic $P2_12_12_1$ symmetry, an intermediate $V = 447$ Å^3 unit cell and intermediate number of Bragg reflexes: 628 observable.
- Poly(ethylene) (PE), as published by Kavesh and Schultz (1970), as an example for a 'high' orthorhombic $Pna2_1$ symmetry, a small $V = 92$ Å^3 unit cell and small number of Bragg reflexes: 119 observable.

Their structure files were curated to a common standard. In particular, the individual atomic displacement factors were removed, to be replaced by a unified and controllable displacement factor k. From each file, a series of crystalline-phase diffractograms $I_c^0(s)$ was simulated, using the parameter-space described in the following, with the individual parameters highlighted in bold font.

We chose the March-Dollase model to simulate the pole densities P of individual reflexes based on preferred orientations within the samples (Dollase 1986; Ida 2013):

$$P(r_{po}, \rho) = \left(r_{po}^2 \cos^2 \rho + r_{po}^{-1} \sin^2 \rho \right)^{-3/2} \tag{14}$$

Here $r_{po} = [0.5, 0.8, 1.0, 1.25, 2]$ are the *preferred orientation parameters*, and ρ is the polar angle between the direction of preferred orientation **p**, and the scattering vector **s**, which in basic Bragg-Brentano geometry corresponds to the direction normal to the sample plane, or equally "to the rotation axis of the spinning attachment of the measurement system." (Ida 2013) Thus, we emulated the typical case, where samples are spun during measurement to reduce the effects of texture within the sample plane.

In this notation, values $r_{po} < 1$ correspond to preferred orientation out of the sample plane, $r_{po} = 1$ to no preferred orientation, and $r_{po} > 1$ to preferred orientation within the sample plane (Dollase 1986). Our choice of unevenly spaced r_{po} is the same as used by Ida (2013) and reflects the non-linear progression of the resulting $P(r_{po}, \rho)$. For preferred orientation to have a specific meaning, a reciprocal space vector of the crystal structure's unit cell must be assigned to **p**. Hence, we calculated three diffractograms per $r_{po} \neq 1$, for each of the lattice planes {100}, {010} and {001}.

As the *lower limits of the cumulative integration range* $s_p^0 = [0.3, 0.6, 0.9]$ Å^{-1}, we used the same limits as Ruland (1961) applied for the upper integration limits s_p in the original segment-wise approach. They appear sensible, considering the analyzed range of $s < 1.3$ Å^{-1} and the ranges of s where strong Bragg reflexes are present.

We chose values of the *averaged crystallite sizes* $\overline{L} = [5, 16, 50]$nm that span the range typically encountered in the simulated materials on a logarithmic scale (Gmach and Van Opdenbosch 2022; Haslböck et al. 2018; Gu et al. 2014). These were realized as a combination of Lorentzian and Gaussian broadening.

The scattering profiles of the amorphous phases $I_{am}^0(s)$ were simulated on the basis of the respective crystalline structures by varying the reflex broadening effects of crystallite sizes and microstrain until they matched recorded reference patterns from amorphous materials. Compared to using recorded profiles, this approach allows to analyze the full range of 2θ and retains the absolute scattered intensities.

The simulated patterns for the entire semicrystalline materials were completed as follows, for *actual mass fraction of the crystalline phase* $x_c^0 = [0.25, 0.5, 0.75]$ and **actual thermal displacement factors** $k^0 = [0, 3, 6]$ Å^2. These x_c^0 represent an evenly spaced sequence to assess the influence of the actual crystallinity on its estimator x_c. The k^0 were chosen because $k = 6$ Å^2 was reported for cellulosic materials (Sao et al. 1994), together with no thermal displacement and an intermediate value.

From the unscaled and unattenuated crystalline-phase diffractograms $I_c^0(s)$, the amorphous scattering profiles $I_{am}^0(s)$, and via Eq. (3), the total coherent and incoherent intensities were calculated by Eqs. (15) and (16), after ensuring that the prerequisite (17) held true:

$$\begin{aligned} I_{coh}(s) &= I_c(s)\, D(s) \\ &= I_c^0(s) x_c D(s) \end{aligned} \tag{15}$$

$$I_{\mathrm{inc}}(s) = I_{\mathrm{am}}(s) \left[1 + \frac{x_{\mathrm{c}}(1 - D(s))}{1 - x_{\mathrm{c}}}\right] = I^0_{\mathrm{am}}(s)(1 - x_{\mathrm{c}})\left[1 + \frac{x_{\mathrm{c}}(1 - D(s))}{1 - x_{\mathrm{c}}}\right] = I^0_{\mathrm{am}}(s)(1 - x_{\mathrm{c}} D(s)) \quad (16)$$

$$\int_0^\infty I^0_{\mathrm{c}}(s)s^2\,\mathrm{d}s = \int_0^\infty I^0_{\mathrm{am}}(s)s^2\,\mathrm{d}s = \int_0^\infty \langle f^2(s)\rangle s^2\,\mathrm{d}s \quad (17)$$

Then, (15) and (16) correspond to (2) and (8) and the simulated observed scattering $I(s) = I_{\mathrm{coh}}(s) + I_{\mathrm{inc}}(s)$. We proceeded to calculate $R(s_p)$ by Eq. (11), determine the fitting function $y(s_p^2)$ to $R(s_p)$ over s_p^2 using a least-squares algorithm, and x_{c} and k via Eqs. (12) and (13).

Hence, we tested 405 parameter sets from a matrix of input parameters $r_{\mathrm{po}} \times s_p^0 \times \overline{L} \times x_{\mathrm{c}}^0 \times k^0$ and their results $x_{\mathrm{c}} \times k$ per polymer and preferred orientation in {100}, {010} and {001}. These were treated in three different manners:

- To answer H1 and to determine the effects of each input parameter per polymer, we plotted the collective results as functions thereof.
- To answer H2 and to determine those input parameters consistently yielding accurate results per polymer, we created violin plots of those fulfilling conditions of accuracy.
- To answer H3 and H4 and to determine the overall effects of each input parameter, we created correlation plots of the input parameters to the absolute deviations of the results.

Results

For each polymer and set of parameters, a composite graph showing the separation of $I(s)$ into $I_{\mathrm{coh}}(s)$ and $I_{\mathrm{inc}}(s)$, as well as into $I_{\mathrm{c}}(s)$, $I_{\mathrm{diff}}(s)$ and $I_{\mathrm{am}}(s)$ was created for quality control. Here, we present typical examples: Fig. 1a shows a single graph without preferred orientation, for a set of parameters typical of cellulose. As anticipated, the method of Ruland and Vonk returns the correct value of x_{c}, Fig. 1b. We note that the returned $k \neq k^0$. All evaluations pertaining to the accuracies of x_{c} were also performed for the k.

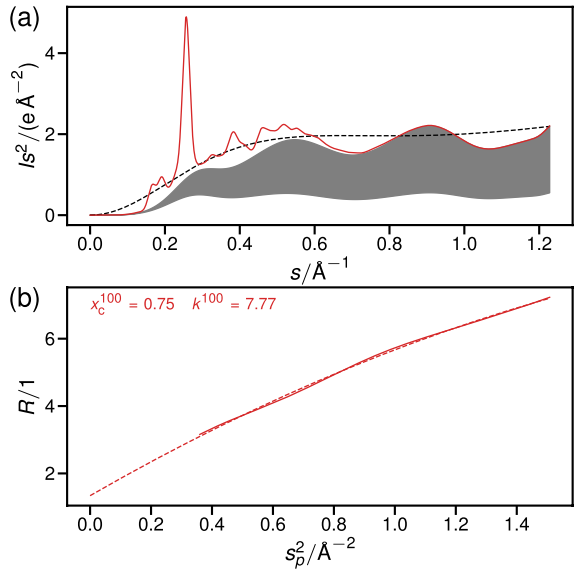

Fig. 1 $I(s)s^2$ in electron units (**a**) and $R(s_p)$ (**b**) for a semicrystalline Cell I α material with the parameters: $r_{\mathrm{po}} = 1$, $s_p^0 = 0.6$ Å^{-1}, $\overline{L} = 5$ nm, $x_{\mathrm{c}}^0 = 0.75$ and $k^0 = 6$ Å^2. In (**a**), the full line marks the progression of $I(s)s^2$, its difference to the gray shaded area is $I_{\mathrm{coh}}(s)s^2$, the gray area itself $I_{\mathrm{diff}}(s)s^2$, and its upper and lower boundaries $I_{\mathrm{inc}}(s)s^2$ and $I_{\mathrm{am}}(s)s^2$. Hence, the difference from the full line to the lower boundary of the shaded area is $I_{\mathrm{c}}(s)s^2$. The dashed line signifies $\langle f^2(s)\rangle s^2$. In (**b**), the results obtained by the method of Ruland and Vonk are shown as an inset

However, for brevity, they are presented as Supporting Information and not discussed in this work.

Figure 2(**a**) shows three graphs with preferred in-plane orientations of the planes {100}, {010} and {001}. The blue line exemplifies the diffractogram typically recorded from non-regenerated cellulosic materials: An in-plane texture of the planes {001}, corresponding approximately to the long axis of the cellulose molecules within the unit cell, a crystallite size in the single-figure nanometer range, a three quarters mass fraction of the crystalline phase and a typical thermal factor. Notably, Fig. 2b shows that the x_{c} from all three simulated preferred orientation directions were within 3 % of the simulated actual value. The corresponding progressions for Cell II, PHB and PE are shown in Figs. 3, 4, 5.

The graphs in Figs. 6, 7, 8, 9,10 are all $x_{\mathrm{c}} - x_{\mathrm{c}}^0$, plotted over each of the assessed parameters, for each of the three simulated directions of preferred orientation and for each of the simulated materials. They

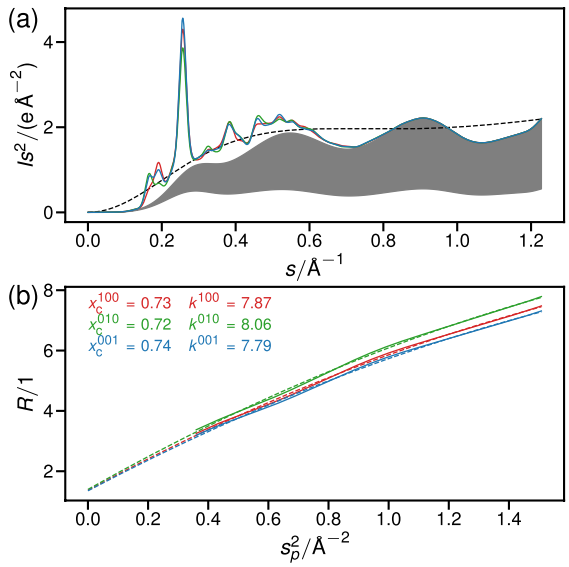

Fig. 2 $I(s)s^2$ in electron units (**a**) and $R(s_p)$ (**b**) for a semicrystalline Cell I α material with the parameters: $r_{po} = 1.25$, $s_p^0 = 0.6$ Å^{-1}, $\overline{L} = 5$ nm, $x_c^0 = 0.75$ and $k^0 = 6$ Å^2 for preferred orientation in {100} (red), {010} (green) and {001} (blue)

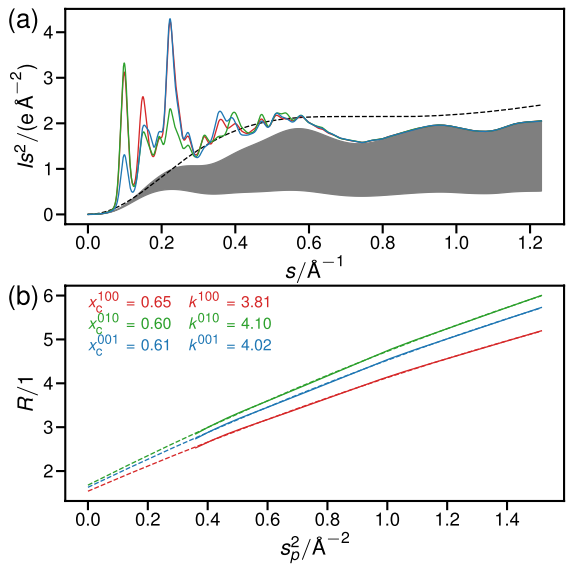

Fig. 3 $I(s)s^2$ in electron units (**a**) and $R(s_p)$ (**b**) for a semicrystalline Cell II material with the parameters: $r_{po} = 1.25$, $s_p^0 = 0.6$ Å^{-1}, $\overline{L} = 5$ nm, $x_c^0 = 0.75$ and $k^0 = 6$ Å^2 for preferred orientation in {100} (red), {010} (green) and {001} (blue)

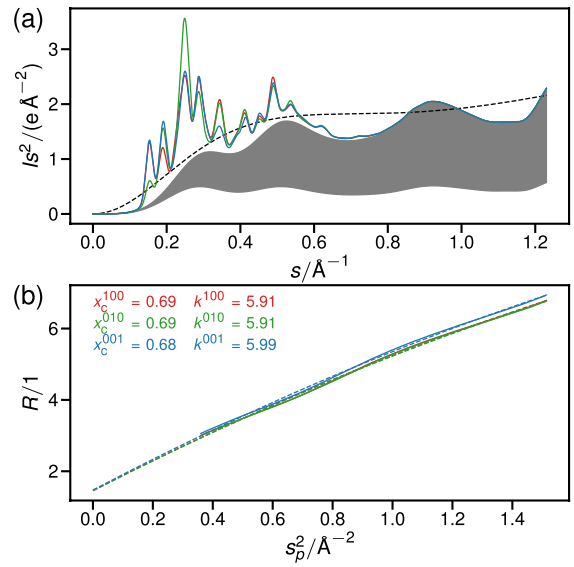

Fig. 4 $I(s)s^2$ in electron units (**a**) and $R(s_p)$ (**b**) for a semicrystalline PHB material with the parameters: $r_{po} = 1.25$, $s_p^0 = 0.6$ Å^{-1}, $\overline{L} = 5$ nm, $x_c^0 = 0.75$ and $k^0 = 6$ Å^2 for preferred orientation in {100} (red), {010} (green) and {001} (blue)

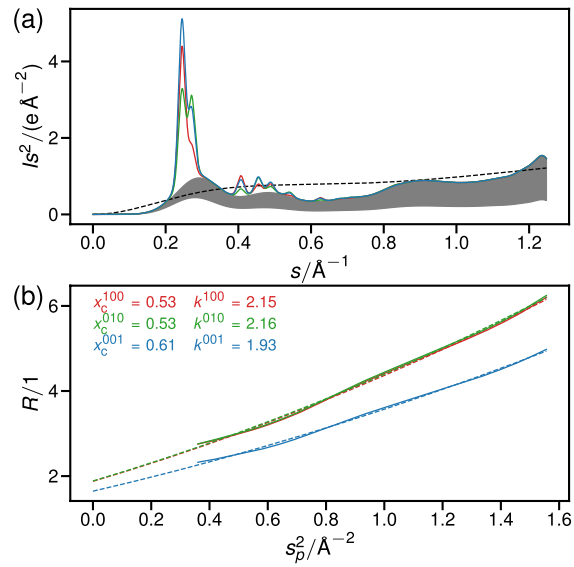

Fig. 5 $I(s)s^2$ in electron units (**a**) and $R(s_p)$ (**b**) for a semicrystalline PE material with the parameters: $r_{po} = 1.25$, $s_p^0 = 0.6$ Å^{-1}, $\overline{L} = 5$ nm, $x_c^0 = 0.75$ and $k^0 = 6$ Å^2 for preferred orientation in {100} (red), {010} (green) and {001} (blue)

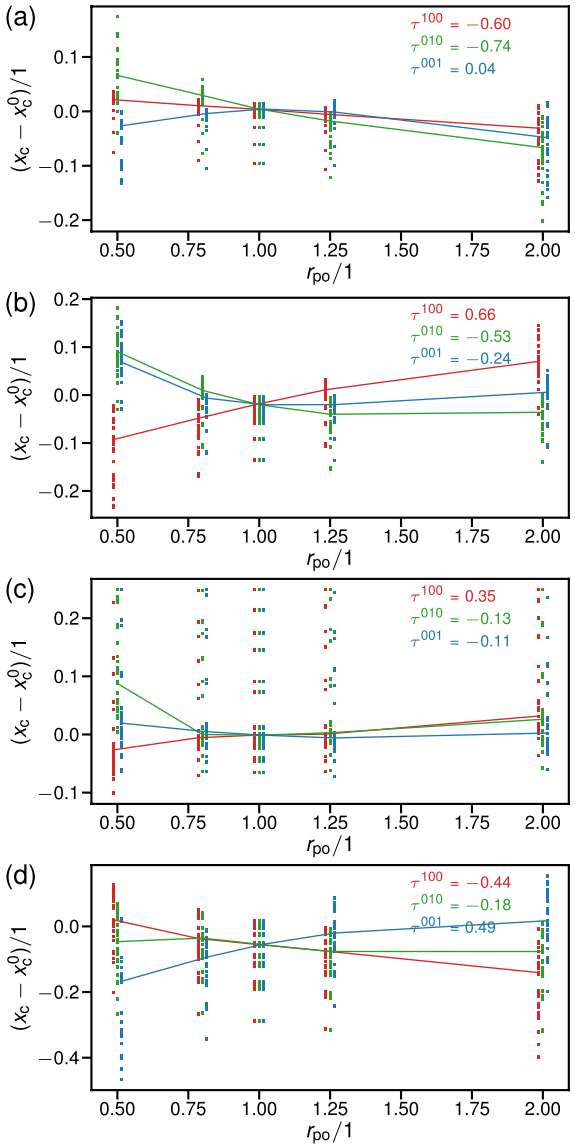

Fig. 6 Deviations of x_c from the actual value x_c^0 as a function of the preferred orientation parameters r_{po} for preferred orientation in {100} (red), {010} (green) and {001} (blue), for semicrystalline Cell I α (**a**), Cell II (**b**), PHB (**c**) and PE (**d**), with correlation coefficients as insets

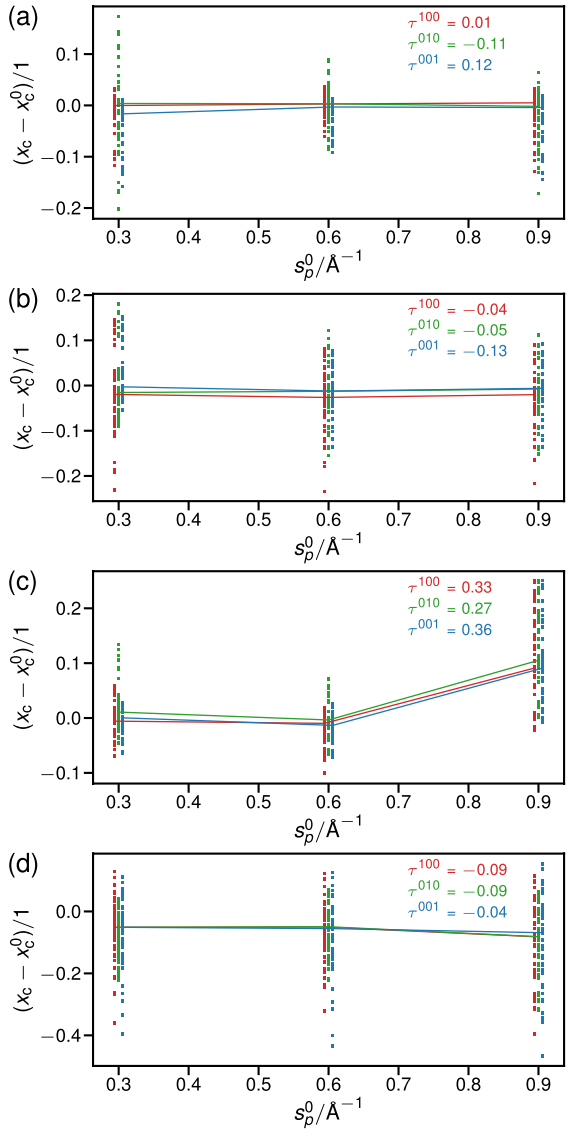

Fig. 7 Deviations of x_c from the actual value x_c^0 as a function of the lower limits of the cumulative integration range s_p^0 for preferred orientation in {100} (red), {010} (green) and {001} (blue), for semicrystalline Cell I α (**a**), Cell II (**b**), PHB (**c**) and PE (**d**), with correlation coefficients as insets

are mirrored for all $k - k^0$ in Supporting Information, Figures S1 to S5. We also plotted lines connecting the median values per data point, and calculated the Kendall τ correlation coefficients of their progressions with the respective parameter.

The graphs in Figs. 11, 12, 13 are violin plots of all values per parameter leading to $|x_c - x_c^0| < \alpha$ for three different α and for each of the simulated materials. They are mirrored for all $|k - k^0| < \alpha$ in Supporting Information, Figures S6 to S8. Per parameter, we distinguished between those values where $|x_c - x_c^0| < \alpha$ for any preferred orientation $\{hkl\}$, and those values where this was true specifically for preferred orientation in {001}.

The correlation plot shown in Fig. 14 was created using all input data from all considered polymers, and

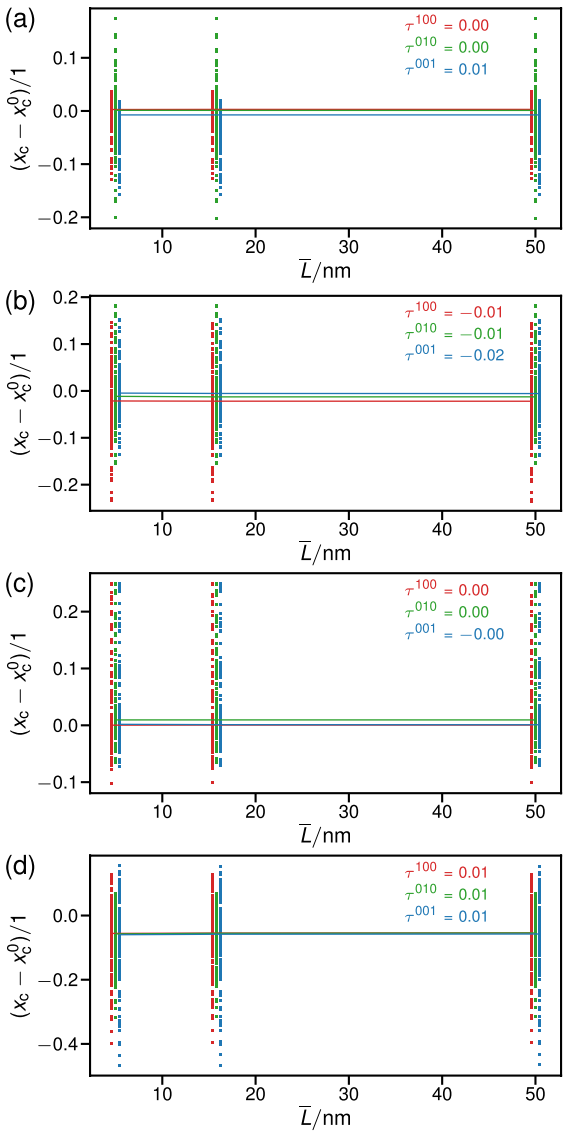

Fig. 8 Deviations of x_c from the actual value x_c^0 as a function of the averaged crystallite sizes $\overline{L}$ for preferred orientation in {100} (red), {010} (green) and {001} (blue), for semicrystalline Cell I α (**a**), Cell II (**b**), PHB (**c**) and PE (**d**), with correlation coefficients as insets

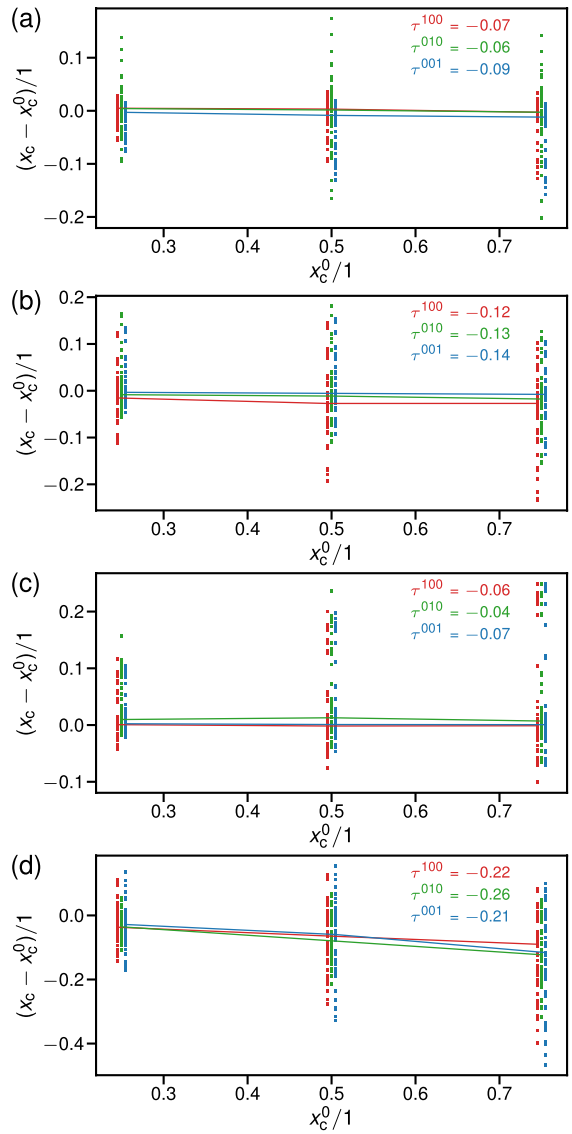

Fig. 9 Deviations of x_c from the actual value x_c^0 as a function of the actual mass fraction of the crystalline phase x_c^0 for preferred orientation in {100} (red), {010} (green) and {001} (blue), for semicrystalline Cell I α (**a**), Cell II (**b**), PHB (**c**) and PE (d), with correlation coefficients as insets

their directional results. The values in the upper left quadrant show the expected non-correlation between the input parameters. Those in the lower right quadrant show that all deviations $x_c - x_c^0$ and $k - k^0$ are positively correlated with one another. The values in the lower left and upper right quadrants show the correlations of interest, between the input parameters and the deviations $x_c - x_c^0$.

Discussion

Errors incurred by preferred orientation

the deviations of the determined x_c from the input values x_c^0 as functions of r_{po} for the three simulated polymers, Fig. 6, and the violin plots (a) in Figs. 11, 12, 13 show that indeed, the higher the crystal symmetry

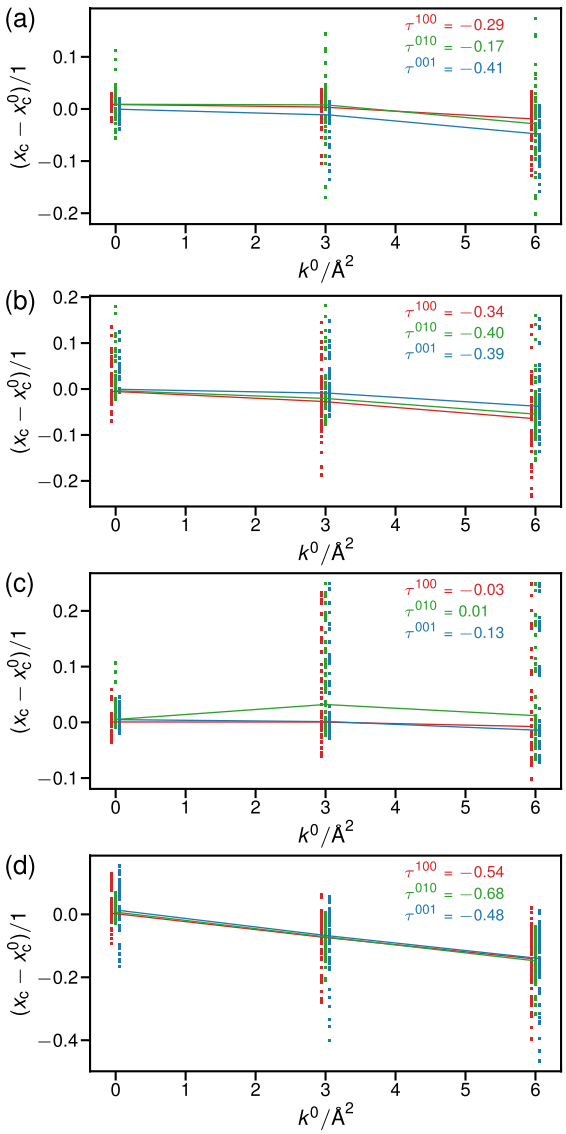

Fig. 10 Deviations of x_c from the actual value x_c^0 as a function of the actual thermal displacement factors k^0 for preferred orientation in {100} (red), {010} (green) and {001} (blue), for semicrystalline Cell I α (**a**), Cell II (**b**), PHB (**c**) and PE (**d**), with correlation coefficients as insets

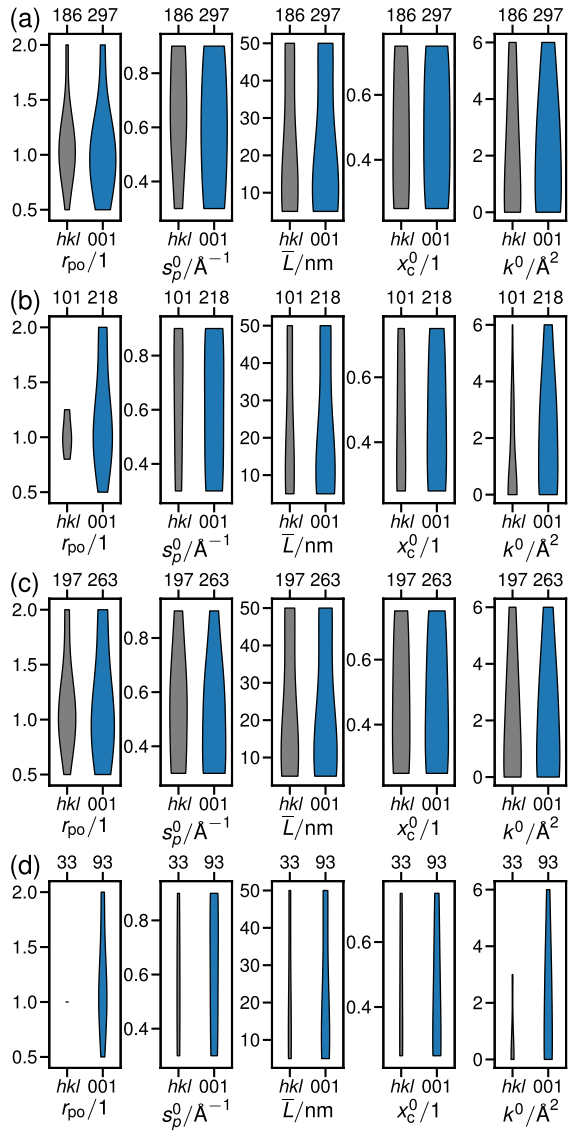

Fig. 11 Violin plots of all parameter values for which $|x_c - x_c^0| < 0.03$ for all preferred orientation directions {*hkl*} and only for {001}, for semicrystalline Cell I α (**a**), Cell II (**b**), PHB (**c**) and PE (**d**). The violin widths are scaled to the number of values out of a total of 405 stated on the upper abszissa

and the lower the unit cell volume and therefore the fewer the number of observed Bragg reflexes, the larger the variances of $x_c - x_c^0$. Notably, this is true for any direction of preferred orientation, and also for any individual r_{po}. Therefore, with the caveat of a limited number of observations, specifically with regard to the number of simulated materials, and without a quantitative statement on the correlation between symmetry and the x_c, we accept hypothesis H1 as true.

Within each material, Figs. 6a–d, the overall most accurate and precise measures x_c are obtained for $r_{po} = 1$. However, for PE, Fig. 6d, the median of these values was at −0.05, indicating a systematic imprecision to lower x_c. This leads the curious finding that for certain amounts and directions of

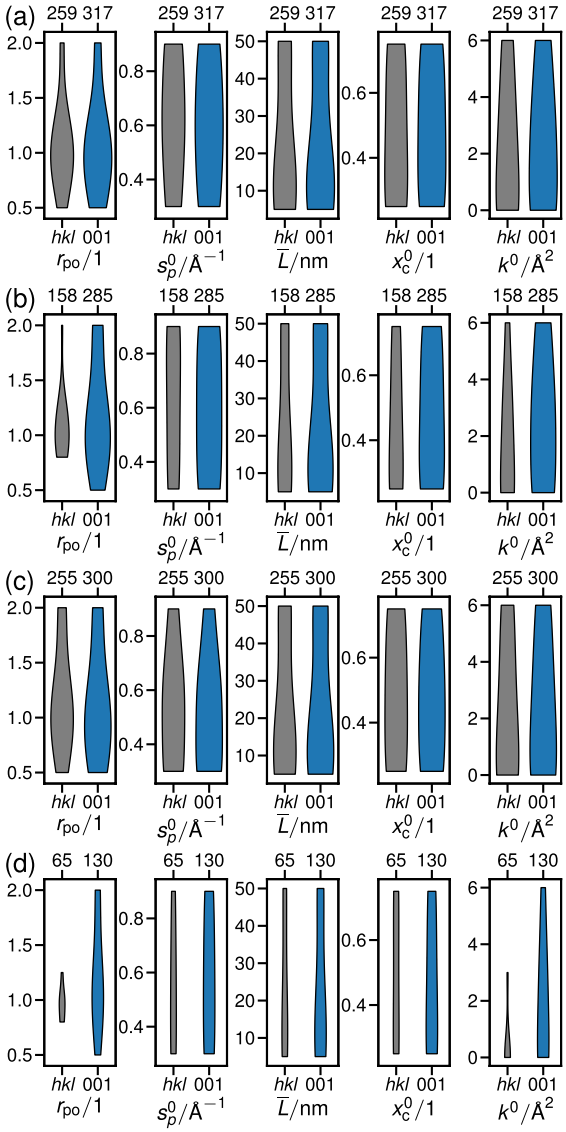

Fig. 12 Violin plots of all parameter values for which $|x_c - x_c^0| < 0.05$ for all preferred orientation directions $\{hkl\}$ and only for $\{001\}$, for semicrystalline Cell I α (**a**), Cell II (**b**), PHB (**c**) and PE (**d**). The violin widths are scaled to the number of values out of a total of 405 stated on the upper abszissa

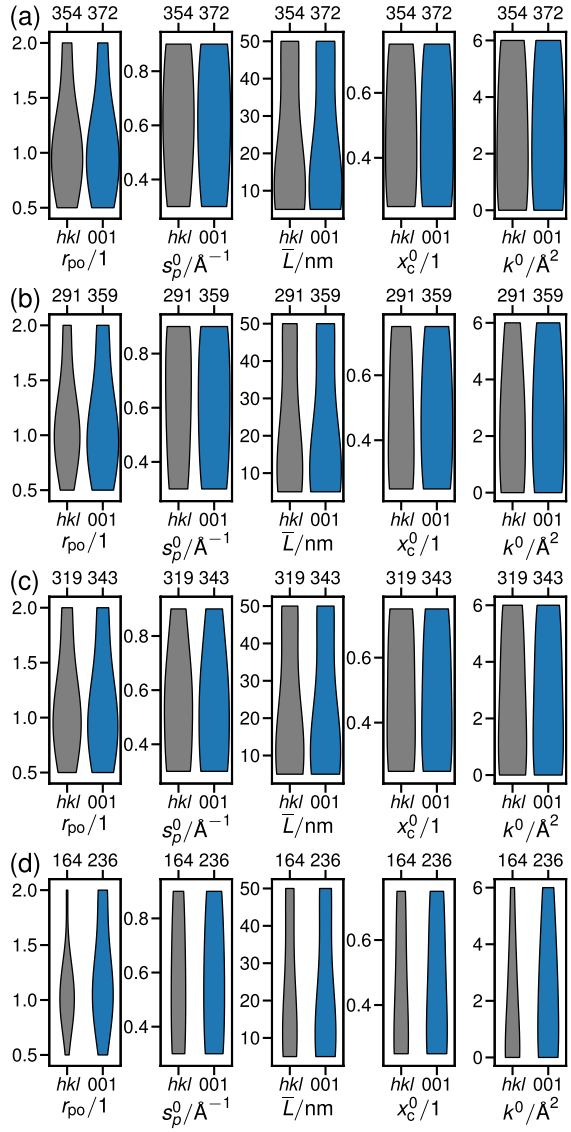

Fig. 13 Violin plots of all parameter values for which $|x_c - x_c^0| < 0.1$ for all preferred orientation directions $\{hkl\}$ and only for $\{001\}$, for semicrystalline Cell I α (**a**), Cell II (**b**), PHB (**c**) and PE (**d**). The violin widths are scaled to the number of values out of a total of 405 stated on the upper abszissa

preferred orientation, similarly accurate (if more imprecise) measures x_c were obtained. The violin plots for different accuracies α in Figs. 11, 12, 13 confirm these findings: For all materials, the most common values leading to $|x_c - x_c^0| < \alpha$ were $0.8 \leq r_{po} \leq 1.25$. But, for PE with texture in $\{001\}$ and $\alpha = 0.1$, a large proportion of accurate values were obtained also for $r_{po} = 2$.

When considering the number of values fulfilling $|x_c - x_c^0| < \alpha$ out of 405 parameter sets per sample, we find that both celluloses and PHB score significantly more hits than PE, upper abszissae in Figs. 11, 12, 13. In PE, only 8 % of the parameter sets yielded the correct values $x_c^0 \pm 3$ % if all possible directions of preferred orientation had to fulfill the condition, and then, only in the absence of texture, as shown by

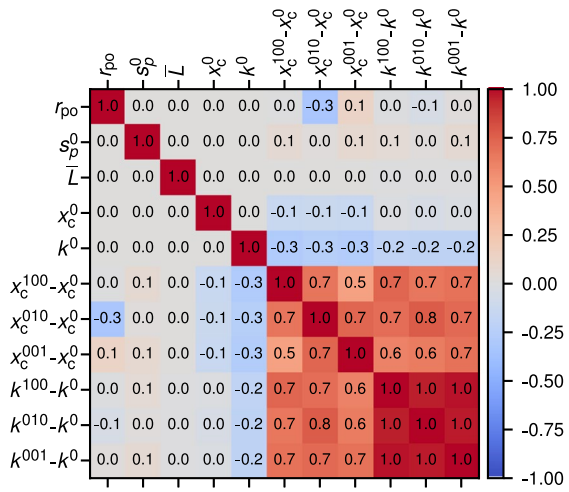

Fig. 14 Correlation matrix of the input parameters, and the deviations of the directional results x_c and k from their input values

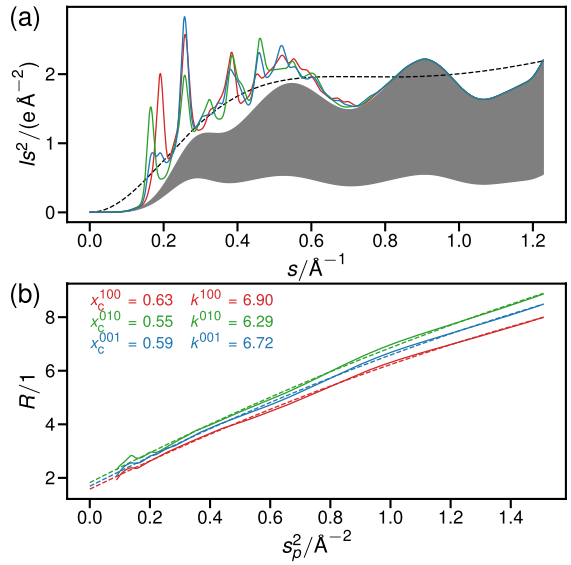

Fig. 15 $I(s)s^2$ in electron units (**a**) and $R(s_p)$ (**b**) for a semicrystalline Cell I α material with the parameters: $r_{po} = 2.00$, $s_p^0 = 0.3$ Å^{-1}, $\overline{L} = 5$ nm, $x_c^0 = 0.75$ and $k^0 = 6$ Å^2 for preferred orientation in {100} (red), {010} (green) and {001} (blue)

the *hkl* column, Fig. 11d. Even if the condition had to be fulfilled only by {001}, a mere 23 % of the values were correct.

It is therefore advisable to determine values of crystallinity obtained for highly symmetric crystalline phases by another means. This is the case for thermoplastics, which typically crystallize in an orthorhombic symmetry, as in the examples of PHB and PE, in which case thermocalorimetry may be considered. In the case of cellulose, one may consider an accuracy of ±10 % satisfactory. There, both Cell I α and Cell II yielded accurate values in at least 72 % of cases (Fig. 13b, *hkl* column), and systematically for $0.5 < r_{po} \leq 1.25$ and the associated pole densities (Dollase 1986; Ida 2013).

On average, a roughly similar number of hits $|x_c - x_c^0| < \alpha$ were scored for $r_{po} = 0.5$ and for $r_{po} = 2$, as discernible from Figs. 11, 12, 13, which can be rationalized as follows: In a basic Bragg-Brentano experiment, the sample normal is close to parallel with the scattering vector, and therefore $\rho \approx 0$. Then, $P(r_{po} = 0.5, \rho = 0) = 8$, and $P(r_{po} = 2, \rho = 0) = 1/8$. In both cases, we had conserved the total intensities by Eq. (17). Hence, these two values of pole density describe a relative intensification or weakening of reflexes arising from a set of lattice planes, by the same multiplier or fraction.

In our application of the March-Dollase model, we assume that all lattice planes perpendicular to the direction of preferred orientation have random orientations. Such uniplanar orientation, $r_{po} > 1$, is the case typically observed in cellulose I α, even though bacterial cellulose may exhibit selective uniplanar orientations in the terminology used by Sisson (Gmach and Van Opdenbosch 2022; Sisson 1935). In the updated terminology by Heffelfinger and Burton (1960), these two phenomena are referred to as planar and uniplanar, respectively.

We note that in cellulose, due its non-orthogonal unit cells, one or more lattice planes are at an angle to the crystal axes. Hence, even in the case of crystal axes being perfectly parallel to the sample plane, directions of preferred orientation **p** may be not. The result is a limit on realistic values of r_{po} for that direction. This leaves open the question: Which values of r_{po} correspond to orientations actually found in cellulosic materials?

Figure 15 shows an example of strong preferred orientation $r_{po} = 2$. Based on our experience with native cellulosic materials with preferred in-plane orientation of the planes {001}, measured patterns are closer to the blue line shown in Fig. 2 where $r_{po} = 1.25$, than to the blue line in Fig. 15. We therefore consider that in this case, $r_{po} > 1.5$ are atypical.

This means that typically, crystallinities determined from cellulosic materials by the method of Ruland and Vonk should not be inaccurate due to the effects of preferred orientation, as confirmed by the 001 columns of the plots (a,b) in Figs. 11, 12, 13.

The low numbers of total hits in Figs. 11d, 12d, 13d suggest that this is not true for PE. This is confirmed by Fig. 6d, where the $x_c - x_c^0$ exhibit much larger variances for any s_p^0. All else having been equal, this must be traced to the differences in crystal structure. The examples shown in Figs. 3, 4, 5 support this notion.

Proper choice of the cumulative integration range

As outlined in the previous section, relative directional intensity changes do influence the overall accuracy of x_c in a systematic manner, which depends on the placement of corresponding reflexes $\{hkl\}$. For example, in Cell I α, the three reflexes with highest intensities are $\{100\}$, $\{010\}$ and $\{110\}$, whereas in Cell II, they are $\{1\bar{1}0\}$, $\{110\}$ and $\{020\}$. These lists are in ascending order of s, which suggests that the choice of s_p^0 –together with the effects of preferred orientation– will influence the results, as hinted at by Vonk (1973): Too high, and the range of s for extrapolation of $y(s_p^2)$ to 0 will be short, and far from its aim point. Too low, and $R(s_p)$ may oscillate strongly, and differently, depending on r_{po}. This is illustrated by Fig. 15, where strong preferred orientations are combined with a low s_p^0. For the same simulated Cell I α, the results using $s_p^0 = 0.6$ Å^{-1} were both more accurate and precise, at $x_c^{100} = 0.69$, $x_c^{010} = 0.66$ and $x_c^{001} = 0.66$. For $s_p^0 = 0.9$ Å^{-1}, they were similarly inaccurate and imprecise as for $s_p^0 = 0.3$ Å^{-1}, at $x_c^{100} = 0.62$, $x_c^{010} = 0.58$ and $x_c^{001} = 0.61$.

The graphs in Fig. 7, showing the values obtained from each single measurement, and the s_p^0 columns in the graphs in Figs. 11, 12, 13 support the finding that $s_p^0 = 0.6$ Å^{-1} is –among the tested values– the lower limit to the range s_p that systematically yields the most accurate x_c. Hence, we accept hypothesis H2 as true.

This finding contradicts the practice of Vonk, who used $s_p^2 = 0.1$ Å^{-2}, corresponding to $s_p^0 \approx 0.3$ Å^{-1} to illustrate the method (Fig. 1 in cited article) (Vonk 1973). It does, however, correspond to the limit used by Vonk (1973) to estimate the inelastic scattering (Fig. 2 in cited article). Hence, $s_p^0 = 0.6$ Å^{-1} provides a good balance between a sufficient overlap of Bragg reflexes to yield a stable function $R(s_p)$, and their remaining intensities and the distance for interpolation.

Influence of the attenuation rate of coherent scattering

We had expected k^0 to influence the accuracy $x_c - x_c^0$: For $k^0 = 0$, $R(s_p)$ oscillates around a constant value. Therefore, the fitting function $y(s_p^2)$ progresses along a constant value, and $x_c \approx 1/y(s_p^2)$ for any value of s_p. With increasing k_0, the function $y(s_p^2)$ is supposed to pivot around $y(0) = 1/x_c$. The results in Figs. 6, 7, 8, 9, 10 suggest that it does so for $r_{po} \approx 1$ and the proper choice of s_p^0. Otherwise, its point of aim wanders, as confirmed by the composite graphs used for quality control (not shown for brevity).

Figure 10 demonstrates that the choice of k^0 indeed correlates with the obtained accuracy $x_c - x_c^0$. Its effect was most striking in PE, Fig. 10d. The observable inverse correlation of k^0 with $x_c - x_c^0$ are also confirmed by Fig. 14. Figures 11 to 13 show that among the tested parameters, and for all materials, the choice of k^0 had the –broadly speaking– second-largest effect on the accuracies of x_c, after r_{po}. Hence, we can accept hypothesis H3 as true.

To answer the 'sub-'hypotheses H3.1 and H3.2, we consider Fig. 14. Here, we find that the correlations of both k^0 and r_{po} with $x_c - x_c^0$ are only similar, and therefore H3.1 true for preferred orientation in $\{010\}$. We find H3.2 to be false.

It should be noted that the exemplary $k = 6$ Å^2, while likely accurate for cellulose, may not apply to other polymers. For example, Vonk determined that 1.1 Å$^2 < k < 3.4$ Å^2 for PE. For this reason, and also for the crystallite sizes, which are typically larger in PE, Fig. 5 may differ in appearance from a measurement.

In the Supporting Information, Figures S1 to S8, we have included a duplicate of the evaluations of $x_c - x_c^0$, shown in Figs. 6, 7, 8, 9, 10, 11, 12, 13, for $k - k^0$. While their discussion is outside the scope of this work, they point to a behaviour that is overall similar to $x_c - x_c^0$.

Effects of crystallite sizes and actual crystallinities

Based on the data and the aforementioned discussion points, we consider the density of observable Bragg

reflexes to be the characteristic most directly determining the reliability of x_c: The higher, the better. This is evident from the comparison between Cell I α, Cell II and PHB, and PE (Figs. 2, 3, 4, 5): The low number of reflexes in PE, leading to low $I_{coh}(s)$ at large s produces a curve $R(s_p)$ that shows oscillations even at large s_p^2.

Varying $\overline{L}$ alter the widths, but not the number and distribution (i.e. density) and integral intensities of Bragg reflexes, while changing x_c^0 alter the integral intensities of Bragg reflexes relative to the total observed intensities, but not relative to one another, and not their density. We therefore did not expect these two parameters to influence the accuracies $x_c - x_c^0$ determined by Ruland and Vonk. Figures 8 and 9 show that this –and therefore also hypothesis H4– is true. We assume that this finding also holds true for anisotropic crystallite sizes.

The above statement seems to be contradicted by the values presented for the dependence of $x_c - x_c^0$ on x_c^0 in PE, Fig. 9d. We speculate that there is generally a cross-correlation between the influences of x_c^0 and k^0. Since in PE, $x_c - x_c^0$ correlates strongly with k^0, this may affect its correlation with x_c^0 no a noticeable degree.

The independence of the results obtained by the method of Ruland and Vonk from $\overline{L}$ is in marked contrast to those obtained by the method of Segal (1959). Here, increasing peak broadening lowers the maximum intensities of Bragg reflexes, and, below a size threshhold, increases the intensities at the midpoints between reflexes. Hence, French and Santiago Cintrón (2013) determined that Segal crystallinity indices drop noticeably below $\overline{L} \approx 7$ nm.

Comments on data collection and treatment

The lower limit s_p^0 to the range s_p may be confused with the lower integration limit s_0. The latter was set to $s_0 = 0.1$ Å^{-1} by Ruland (1961), and to $s_0 := 0$ by Vonk (1973) and in this work. In Ruland's work, this was obviously chosen to provide uniform lower bounds for the individual intervals $[s_0;s_p]$ while excluding intensities stemming from the setup. In Vonk's adaptation, using cumulative integration of $I(s)$ and $I_{coh}(s)$ from s_0 to obtain $R(s_p)$ over the interval $[s_p^0;s_p]$ made fixing the lower bound to a specific and uniform value unnecessary, hence the blanket statement $s_0 := 0$.

This does not mean that it should not be considered. In practice, the lower bound s_0 is never 0, but defined by the lower limit of the assessed data range. The graphs (a) in Figs. 1, 2, 3, 4, 5 show that below $s \approx 0.1$ Å^{-1}, which translates to $2\theta \approx 9°$ with copper Kα $_1$ radiation, $I(s)s^2$ is negligibly small. Carefully choosing the lower limit of the assessed data range may also lessen errors incurred by scattering from the setup. While the direct beam typically becomes visible only below $2\theta \approx 2°$, air-scattering, while effectively reducible by slits or screens, may be recorded at higher angles. We therefore consider Ruland's original choice of $s_0 = 0.1$ Å^{-1} a good de facto lower bound for most polymers.

The accessible upper bound of the range s_p is defined by the X-ray wavelength and the maximum measurable scattering angle $2\theta \leq 180°$. When simulating data, where the number of data points is only limited by the computer performance, this limit is the sole effect of a choice of wavelength (in recorded data, the data points are limited by the goniometer precision). We know of no argument for artificially truncating the upper limit of the range s_p when performing the method of Ruland and Vonk.

The correction for the sample holder has the potential to introduce systematic errors. In our experience, holders not exhibiting Bragg reflexes (e.g. specifically cut silicon) are particularly treacherous: An accurate correction requires not only the collection of a blank scan from the holder, but also to estimate the beam attenuation through the sample during the actual measurement. In holders showing Bragg reflexes, the attenuation can be estimated by the reduction of their integral intensities, allowing to scale the corresponding blank scan for subtraction from the measured data.

In this work, the diffractograms were simulated, and therefore readily separated into $I_{coh}(s)$ and $I_{inc}(s)$. The method of Ruland and Vonk allows to determine crystallinities on their basis, without the need to deconvolve the background $I_{inc}(s)$. Straightforwardly, the crystalline peaks may be separated from the continuous background by a smooth function, e.g. a spline. Vonk (1973) pointed out that in this approach, one has to assume that the intensities $I_{coh}(s)$ go to 0 between reflexes, providing knots for the background

function. The graphs in Figs. 1, 2, 3, 4, 5 show that this is rarely true.

For this reason, we consider it advisable to separate recorded $I(s)$ by a Rietveld refinement. This ensures that the attenuation of Bragg peak intensities is modeled by a physically plausible function $D(s)$. At this point, machine-specific influences outside the scope of this article, such as variable slits or monochromators may require data pre-treatment or be part of the machine description during refinement. A Rietveld refinement has the additional advantage of yielding further structural information, most importantly also on the preferred orientation and the progression of Bragg peak attenuation. These, in turn may be used to identify possible causes of errors for x_c.

The equations governing the pole densities $P(r_{po}, \rho)$ are different for transmission measurements (Ida 2013), which, if available, is a popular option for highly transmissive materials such as cellulose. Here, the method of Ruland and Vonk can be applied without modifications, as demonstrated by Fink et al. (1985). However, while the transmission case can be modeled by typical Rietveld refinement routines, values of r_{po} must be converted for comparison to those presented here.

In practice, and depending on the material and the Laue class, more complicated expressions of preferred orientation than expressable by the March-Dollase model may arise. In the material of interest in this work, cellulose, this case appears in bacterial cellulose, where spherical harmonic functions can be applied to model the directional intensities during Rietveld refinement (Gmach and Van Opdenbosch 2022). We suggest that resulting values of pole density may be compared to the corresponding March-Dollase parameters r_{po} to estimate the influence of preferred orientation.

Unraveling multiple crystalline phases

Demonstrably, for many types of polymers and over a wide field of structural parameters, the method of Ruland and Vonk will yield values of crystallinity that are accurate to within ±5 %. Another matter is the presence of materials composed of more than two phases, which we briefly comment on, depending on the case:

In case of a homogeneous material exhibiting more than one crystalline phase (e.g. partially regenerated cellulose sheets containing cellulose I and II), determining their individual x_c can be achieved straightforwardly by multiphase Rietveld refinement, and the application of the method of Ruland and Vonk to their respective $I_{coh}(s)$ against the total $I(s)$.

In case of a heterogeneous material exhibiting more than one crystalline phase, three cases must be considered:

1. The simplest case is when the weight averaged atomic numbers $\langle Z \rangle$ of all constituents, which for X-rays correspond linearly to the atomic scattering factors, are similar. Then, the material may be treated in the same manner as a homogeneous one to determine the x_c of the individual crystalline phases. In a material of unknown overall composition, this approach does not provide the composition of the amorphous phase.
2. The next complication is given by dissimilar atomic numbers of the constituents, but where it is known that all but one constituent crystallize completely. Vonk and Fagherazzi (1983) covered this case for a two-phase material where the amorphous and crystalline phases have different, but known, compositions. They suggested the application of correction factors $\langle Z_t \rangle / \langle Z_c \rangle$ for accurate values of crystallinity. This approach should be extendable to a larger number of phases, if their $I_{coh}(s)$ can be separated by Rietveld refinement.
3. The final complication is a mixture of semicrystalline constituents of dissimilar atomic numbers. While the relative amounts of the crystalline phases may be determined directly by Rietveld refinement, we consider the composition of the amorphous phase, and therefore also the x_c irresolvable by XRD.

Another approach to solve case #2 consists of two steps: First the mass ratios between the crystalline phases are determined by Rietveld refinement. Then, the method of Ruland and Vonk is applied to the $I^i_{coh}(s)$ assigned to the semicrystalline constituent i. Replacing $I(s)$ in Eq. (11) with $I^i_{coh}(s) + I_{inc}(s)$ for the calculation of $R(s_p)$ yields its crystalline to amorphous mass ratio. From these, the entire composition can be resolved.

Outlook

For typical conditions, the method of Ruland and Vonk yields satisfactorily accurate measures of crystallinities for cellulose. This statement cannot be automatically extended to polymers exhibiting higher crystalline symmetries and therefore smaller numbers of Bragg reflexes. The testing routine used in this work, written in Python, may be used to assess the accuracy of obtained $x_c - x_c^0$ of any crystalline structure of interest, provided structural information in Crystallographic Information File format. It is made available together with an implementation of the method of Ruland and Vonk (Van Opdenbosch 2022).

In biological materials, the water contents of the sample should be considered. Knowledge that the scattering invariant $\int \langle f^2(s) \rangle s^2 \mathrm{d}s$ per unit of mass is higher for water than for cellulose molecules by a factor of 1.16 enables accurately correcting obtained crystallinities. One such correction was proposed by Driemeier and Calligaris (2011), using a coefficient of $1.2 \approx 1.16$.

Due to the systematic influences outlined in this work, the key to being able to accept values of crystallinity returned by the method of Ruland and Vonk as accurate lies outside the evaluation method itself. For example, a diffractogram recorded in standard Bragg-Brentano geometry and evaluated by Rietveld refinement may indicate very strong preferred orientation in the sample. If not, the method of Ruland and Vonk will most likely return an accurate value x_c. If so, a goniometer mount may allow to record and randomize data from different scattering vectors $\mathbf{s}$, then returning to the method. When using an area detector instead, it may be recommended to use a shorter wavelength than copper $\mathrm{K}\alpha_1$, in order to record a sufficient range of s beyond the prominent Bragg peaks.

Acknowledgments The author acknowledges the in-depth discussions during publication processes with Cellulose as a source of inspiration and improvement.

Author Contributions DVO wrote the evaluation algorithm and the manuscript.

Funding Open Access funding enabled and organized by Projekt DEAL. Funding by the German Science Foundation (DFG) via grant VA 1349/5 is gratefully acknowledged.

Availability of data and materials All data and materials is available directly from the author, or via an online repository (Van Opdenbosch 2022).

Declarations

Conflict of interest The author has no competing interests as defined by Springer, 764 or other interests that might be perceived to influence the re765 sults and/or discussion reported in this paper.

Consent to participate No humans or animals, apart from the author, participated in the study at hand.

Consent for publication All data was created by the author, who consents to its publication.

References

Clark GL (1930) Cellulose as it is completely revealed by X-rays. Special application to the growth and classification of cotton, the structure of wood, and the manufacture of rayon. Ind Eng Chem 22(5):474–487

Debye P (1913) Interferenz von Röntgenstrahlen und Wärmebewegung. Annalen Physik 348(1):49–92

Dollase W (1986) Correction of intensities for preferred orientation in powder diffractometry: application of the march model. J Appl Crystallogr 19(4):267–272

Driemeier C, Calligaris GA (2011) Theoretical and experimental developments for accurate determination of crystallinity of cellulose I materials. J Appl Crystallogr 44(1):184–192

Fink HP, Fanter D, Philipp B (1985) Röntgen-Weitwinkeluntersuchungen zur übermolekularen Struktur beim Cellulose-I-II-Phasenübergang. Acta Polym 36(1):1–8

French AD (2014) Idealized powder diffraction patterns for cellulose polymorphs. Cellulose 21(2):885–896

French AD, Santiago Cintrón M (2013) Cellulose polymorphy, crystallite size, and the segal crystallinity index. Cellulose 20(1):583–588

Gehman S, Field J (1939) An X-ray investigation of crystallinity in rubber. J Appl Phys 10(8):564–572

Gmach Y, Van Opdenbosch D (2022) Structural and mechanical anisotropy in rheotactically aligned bacterial cellulose. Cellulose pp 1–17

Gu J, Xu H, Wu C (2014) Thermal and crystallization properties of HDPE and HDPE/PP blends modified with DCP. Adv Polymer Technol 33(1)

Haslböck M, Klotz M, Steiner L, Sperl J, Sieber V, Zollfrank C, Van Opdenbosch D (2018) Structures of mixed-tacticity polyhydroxybutyrates. Macromolecules 51(14):5001–5010

Heffelfinger C, Burton R (1960) X-ray determination of the crystallite orientation distributions of polyethylene terephthalate films. J Polym Sci 47(149):289–306

Ida T (2013) Effect of preferred orientation in synchrotron X-ray powder diffraction. Nagoya Institute of Technology, Annual Report of the Advanced Ceramics Research Center

Kavesh S, Schultz J (1970) Lamellar and interlamellar structure in melt-crystallized polyethylene. I. Degree of crystallinity, atomic positions, particle size, and lattice disorder of the first and second kinds. J Polymer Sci Part A-2 Polymer Phys 8(2):243–276

Kriegner D, Wintersberger E, Stangl J (2013) xrayutilities: a versatile tool for reciprocal space conversion of scattering data recorded with linear and area detectors. J Appl Crystallogr 46(4):1162–1170

Riello P (2004) Quantitative analysis of amorphous fraction in the study of the microstructure of semi-crystalline materials. In: Diffraction analysis of the microstructure of materials, Springer, pp 167–184

Ruland W (1961) X-ray determination of crystallinity and diffuse disorder scattering. Acta Crystallogr A 14(11):1180–1185

Sao K, Samantaray B, Bhattacherjee S (1994) X-ray study of crystallinity and disorder in ramie fiber. J Appl Polym Sci 52(12):1687–1694

Segal L, Creely JJ, Martin A Jr, Conrad C (1959) An empirical method for estimating the degree of crystallinity of native cellulose using the x-ray diffractometer. Text Res J 29(10):786–794

Sisson WA (1935) X-ray studies of crystallite orientation in cellulose fibers. II. Synthetic fibers from bacterial cellulose membranes. Div Cellul Chem, Am Chem Soc 89:343–359

Thygesen A, Oddershede J, Lilholt H, Thomsen AB, Ståhl K (2005) On the determination of crystallinity and cellulose content in plant fibres. Cellulose 12(6):563–576

Van Opdenbosch D (2022) Python implementation of, and evaluation routines for, the method of Ruland and Vonk. https://github.com/Daniel-VO/XRD

Vonk C, Fagherazzi G (1983) The determination of the crystallinity in glass-ceramic materials by the method of ruland. J Appl Crystallogr 16(2):274–276

Vonk CG (1973) Computerization of ruland's x-ray method for determination of the crystallinity in polymers. J Appl Crystallogr 6(2):148–152

Wang H, Tashiro K (2016) Reinvestigation of crystal structure and intermolecular interactions of biodegradable poly (3-hydroxybutyrate) α-form and the prediction of its mechanical property. Macromolecules 49(2):581–594

Yao W, Weng Y, Catchmark JM (2020) Improved cellulose X-ray diffraction analysis using Fourier series modeling. Cellulose 27(10):5563–5579